Dalton Transactions

PAPER

View Article Online
View Journal | View Issue

Cite this: *Dalton Trans.*, 2019, **48**, 14724

The role of neutral Rh(PONOP)H, free NMe_2H, boronium and ammonium salts in the dehydrocoupling of dimethylamine-borane using the cationic pincer $[Rh(PONOP)(\eta^2\text{-}H_2)]^+$ catalyst†‡

E. Anastasia K. Spearing-Ewyn,[a] Nicholas A. Beattie,[b] Annie L. Colebatch,[a] Antonio J. Martinez-Martinez,[a] Andrew Docker,[a] Timothy M. Boyd,[a] Gregg Baillie,[b] Rachel Reed,[b] Stuart A. Macgregor *[b] and Andrew S. Weller *[a]

The σ-amine-borane pincer complex $[Rh(PONOP)(\eta^1\text{-}H_3B{\cdot}NMe_3)][BAr^F{}_4]$ [**2**, PONOP = κ^3-NC_5H_3-2,6-$(OP^tBu_2)_2$] is prepared by addition of $H_3B{\cdot}NMe_3$ to the dihydrogen precursor $[Rh(PONOP)(\eta^2\text{-}H_2)][BAr^F{}_4]$, **1**. In a similar way the related $H_3B{\cdot}NMe_2H$ complex $[Rh(PONOP)(\eta^1\text{-}H_3B{\cdot}NMe_2H)][BAr^F{}_4]$, **3**, can be made *in situ*, but this undergoes dehydrocoupling to reform **1** and give the aminoborane dimer $[H_2BNMe_2]_2$. NMR studies on this system reveal an intermediate neutral hydride forms, Rh(PONOP)H, **4**, that has been prepared independently. **1** is a competent catalyst (2 mol%, ~30 min) for the dehydrocoupling of $H_3B{\cdot}Me_2H$. Kinetic, mechanistic and computational studies point to the role of NMe_2H in both forming the neutral hydride, *via* deprotonation of a σ-amine-borane complex and formation of aminoborane, and closing the catalytic cycle by reprotonation of the hydride by the thus-formed dimethyl ammonium $[NMe_2H_2]^+$. Competitive processes involving the generation of boronium $[H_2B(NMe_2H)_2]^+$ are also discussed, but shown to be higher in energy. Off-cycle adducts between $[NMe_2H_2]^+$ or $[H_2B(NMe_2H)_2]^+$ and amine-boranes are also discussed that act to modify the kinetics of dehydrocoupling.

Received 17th August 2019,
Accepted 3rd September 2019

DOI: 10.1039/c9dt03358k

rsc.li/dalton

Introduction

The dehydrocoupling of amine-boranes, $H_3B{\cdot}NRR'H$ (R, R′ = H, alkyl), is an efficient way to produce new molecules and materials with B–N bonds, with hydrogen as the only by-product.[1–5] Catalytic routes, mainly mediated by transition metal complexes, offer the possibility to influence kinetics and product distributions. This is especially important for the controlled dehydropolymerisation[6–11] of primary amine-boranes, prototypically $H_3B{\cdot}NMeH_2$, that form polymeric materials with main-chain B–N units, $(BHNMe)_n$, that are isosteres of polyolefins and precursors to BN-containing materials.[12–14] Challenges remain,[15] in determining the precise mechanism of dehydropolymerisation which, at the current level of understanding, appears to be a complex and nuanced process. These are exemplified by: (i) the low catalyst loadings required to selectively produce polymers that hamper speciation studies, (ii) polymeric material that becomes insoluble at high molecular weight or with cross-linking, (iii) complex kinetics that often involve induction periods and modification by the hydrogen co-product, (iv) apparent changes in the precise mechanism dependent on the identity of the precatalyst, and (v) a general overarching process that requires two elementary transformations that need to work in concert: dehydrogenation of amine-borane to aminoborane and subsequent controlled polymerisation (Scheme 1).

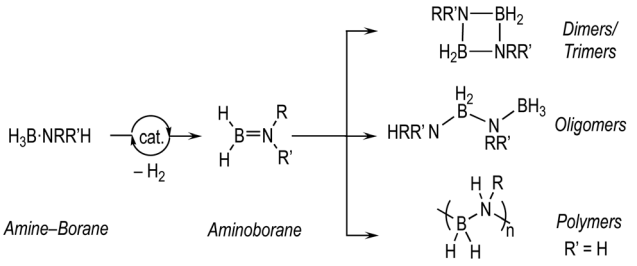

Scheme 1 Generalised dehydrocoupling of methyl amine-boranes. R = H or Me.

[a]*Chemistry Research Laboratories, Department of Chemistry, University of Oxford, Oxford, OX1 3TA, UK. E-mail: andrew.weller@chem.ox.ac.uk*
[b]*Institute of Chemical Sciences, Heriot Watt University, Edinburgh EH14 4AS, UK. E-mail: S.A.Macgregor@hw.ac.uk*

†Dedication: In recognition of Professor Robin N. Perutz's outstanding scientific contributions to physical organometallic chemistry, and also the mentoring and friendship RNP has generously shared with SAM and ASW over their careers.

‡Electronic supplementary information (ESI) available: Synthesis, characterisation data, structures of **2** and **4**, computational details. CCDC 1917326 and 1917160. For ESI and crystallographic data in CIF or other electronic format see DOI: 10.1039/c9dt03358k

The dehydrocoupling of the secondary amine-borane $H_3B{\cdot}NMe_2H$ offers a more straightforward platform to study these processes as the product is a simple soluble dimer, $[H_2BNMe_2]_2$ (Scheme 1), and selectivity for its formation is generally less strongly influenced by catalyst loading, meaning that catalyst speciation and kinetics are easier to study using techniques such as NMR spectroscopy. This provides opportunities to study, in closer detail, the elementary processes occurring in dehydrocoupling, with the caveat that the extra *N*-methyl group may influence both the kinetics and speciation of the catalyst when compared with $H_3B{\cdot}NMeH_2$.[16,17]

Fundamental to any mechanism for dehydrocoupling is the initial dehydrogenation step to form an aminoborane *via* BH/NH activation and loss of H_2. Depending on the catalyst system a number of different routes have been proposed to operate for this, that all invoke σ-amine-borane complexes[18,19] as early intermediates (Scheme 2): (i) step-wise, or concerted, inner sphere;[17,20–22] (ii) ligand-assisted cooperation;[23–26] and (iii) hydride transfer to form a boronium[27] cation that reprotonates the transiently formed hydride.[28–31]

The initial reports of dehydropolymerisation of $H_3B{\cdot}NMeH_2$ used the neutral pincer catalyst $Ir(POCOP)H_2$[7,8,16] [**A**, POCOP = κ^3-C_6H_3-2,6-$(OP^tBu_2)_2$], Scheme 3. A number of closely related pincer-based systems have since been used to catalyse amine-borane dehydrocoupling.[21,26,32–35] However to date no σ-amine-borane complexes have been reported with such systems, despite their key role in catalysis. Related off-cycle products have been characterised.[36] Analogous POP ligand complexes (POP = *e.g.* Xantphos) have a richer coordination chemistry with amine-boranes, and η^1 (*e.g.* **B**) and η^2:η^2-systems have been characterised that are also relevant to the dehydrocoupling of amine-boranes[30,37,38] – although they may not actually lie on the catalytic cycle.[11] For POCOP or PONOP-type systems the preparation, and deployment in catalysis, of a σ-amine-borane complex would provide valuable insight into the mechanism of dehydrocoupling.

We now report that by use of the readily prepared cationic-precatalyst $[Rh(PONOP)(\eta^2\text{-}H_2)][BAr^F{}_4]$[39] [**1**, Ar^F = 3,5-$(CF_3)_2C_6H_3$, PONOP = κ^3-NC_5H_3-2,6-$(OP^tBu_2)_2$] a σ-amine-borane pincer complex can be prepared. **1** is also a competent catalyst for the dehydrocoupling of $H_3B{\cdot}NMe_2H$, and detailed mechanistic studies probe the potential roles of amine (NMe_2H), boronium ($[H_2B(NMe_2H)_2]^+$), ammonium ($[NMe_2H_2]^+$) and a neutral Rh-hydride species in catalytic turnover. The importance of boronium and neutral hydride intermediates in the dehydrocoupling of $H_3B{\cdot}NMe_2H$ was first reported by Conejero and co-workers in cationic Pt-based systems.[28] Hydride transfer from amine-boranes to cationic metal centres has been reported, for example, by Peruzzini[40] and Jagirdar.[41]

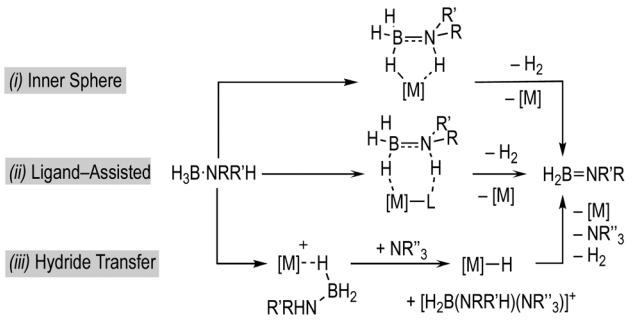

Scheme 2 Generic amine-borane dehydrogenation pathways at a metal centre. The structures of the intermediates are illustrative and do not necessarily capture the order of elementary mechanistic steps for each isolated event.

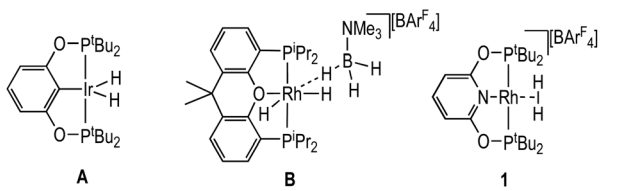

Scheme 3 Examples of pincer complexes used in amine-borane dehydrocoupling and complex **1** used in this contribution.

Results and discussion

Synthesis, structures and reactivity of $[Rh(PONOP)(H_3B{\cdot}NMe_2R)][BAr^F{}_4]$ R = Me, 2; H, 3

Dihydrogen σ-complexes offer convenient entry-points into amine-borane coordination chemistry, as the H_2 ligand is readily displaced.[42–45] The dihydrogen complex $[Rh(PONOP)(\eta^2\text{-}H_2)][BAr^F{}_4]$, **1**, is prepared as a microcrystalline powder[39] from addition of $Na[BAr^F{}_4]$[46] to Rh(PONOP)Cl[47] under an atmosphere of H_2 in CH_2Cl_2 solution followed by recrystallisation. Addition of one equivalent of $H_3B{\cdot}NMe_3$ to **1** in 1,2-$F_2C_6H_4$ solution resulted in displacement of H_2 and the formation in quantitative yield by NMR spectroscopy of $[Rh(PONOP)(\eta^1\text{-}H_3B{\cdot}NMe_3)][BAr^F{}_4]$, **2** (Fig. 1). Recrystallisation of this solution from pentane afforded dark yellow crystals suitable for single crystal X-ray diffraction. The tertiary amine-borane $H_3B{\cdot}NMe_3$ was used in these initial studies to stop onward dehydrocoupling by BH/NH activation.

The solid-state structure of the cationic portion of **2** is shown in Fig. 1. The hydrogen atoms associated with the boron were located and refined. The structure demonstrates an η^1-bound $H_3B{\cdot}NMe_3$ ligand, rather than bidentate η^2:η^2, as determined by a long Rh···B distance [2.567(5) Å] and a rather open Rh–H–B angle [121(4)°].[48,49] There is one closer Rh–H distance [H1, 1.72(5) Å], with the other two considerably distant [2.8–2.9 Å]. In comparison, a pincer complex with a η^2:η^2 $H_3B{\cdot}NMe_3$ bonding mode, $[Rh(NNN)(H_3B{\cdot}NMe_3)][BAr^F{}_4]$ [NNN = 2,6-bis-[1-(2,6-diisopropylphenylimino)ethyl]pyridine] **C**, shows a closer Rh···B distance [2.305(5) Å] and more acute Rh–H–B angles [93(3)°], Scheme 4.[38] Complex **2** is more closely related to $[Ir(POCOP)(H)_2(\eta^1\text{-}HSiEt_3)][B(C_6F_5)_4]$, **D**,[50] which has a far more pronounced η^1 binding mode [Ir···Si 3.346(1) Å, Ir–H–Si 157°], as well as $[Pt(I^tBu')(I^tBu)(\eta^1\text{-}H_3B{\cdot}pyridine)][BAr^F{}_4]$,

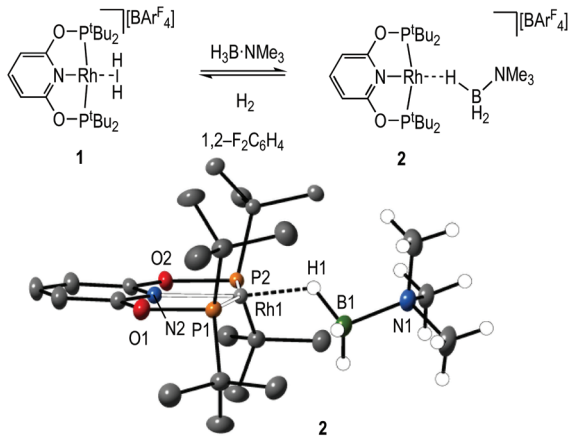

Fig. 1 Synthesis and solid-state structure of complex **2**. Displacement ellipsoids shown at the 30% level. $[BAr^F_4]^-$ anion and most H-atoms are not shown for clarity. Selected bond distances (Å) and angles (°): Rh1–B1, 2.567(5); Rh1–P1, 2.2832(9); Rh1–P2, 2.2594(9); Rh1–N2, 2.026(3); B1–N1, 1.631(6); Rh1–H1, 1.72(5); P1–Rh1–P2, 161.63(3); N2–Rh1–H1, 172.6(17); Rh1–H1–B1, 121(4).

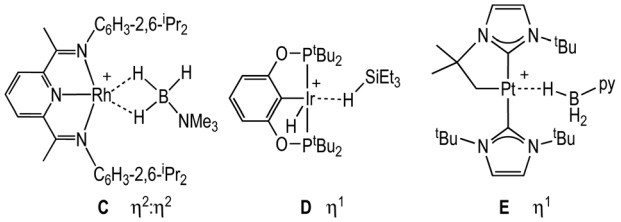

Scheme 4 Comparison of η^1 and $\eta^2{:}\eta^2$ amine-borane and silane complexes.

E [Pt···B 2.8436(5) Å, Pt–H–B 147(4)°][51] (I^tBu = 1,3-di-*tert*-butylimidazolylidene).

Solution NMR spectroscopic data are in agreement with the η^1-binding of the amine-borane being retained in CD_2Cl_2. In the 298 K ^1H NMR spectrum a broad signal integrating to 3 H is observed at δ −2.55 that sharpens on decoupling ^{11}B, that does not change on cooling to 173 K and no coupling to ^{103}Rh is observed. This is indicative of a rapid exchange between terminal and bridging B–H positions.[52,53] A single ^{t}Bu environment was also observed. In the ^{11}B NMR spectrum a broad signal at δ −15.2 that is assigned to the $H_3B{\cdot}NMe_3$ group is shifted 7.9 ppm upfield from free $H_3B{\cdot}NMe_3$ (δ −7.3). The $^{31}P\{^1H\}$ NMR spectrum displays a single doublet at δ 208.9 [J(RhP) = 142 Hz]. Electrospray-Ionisation Mass Spectrometry (ESI-MS) shows the correct isotope pattern for the cation (m/z = 575.26, calc. 575.26). Complex **2** is stable in $1,2\text{-}F_2C_6H_4$ solution for at least 24 hours.

H_2 is a competitive ligand with $H_3B{\cdot}NMe_3$ for coordination at the $\{Rh(PONOP)\}^+$ fragment, and placing a sample of **2** (8.7 mM, $1,2\text{-}F_2C_6H_4$) under 4 atm H_2 in a sealed NMR tube immediately results in a 4 : 1 ratio of **1** : **2** and free $H_3B{\cdot}NMe_3$ – which is now observed as a sharp quartet in the ^{11}B NMR spectrum. Degassing returns **2** as the major component showing that these two species are in equilibrium (Fig. 1). These experimental results are consistent with a computed ΔG from DFT calculations (see later) that is close to thermoneutral, being −1.2 kcal mol^{-1} in favour of **2**. Under a D_2 atmosphere (1 atm) H/D exchange at the borane also occurs, to afford the H_2-, HD- and D_2-isotopologues of **1**, as identified by their distinctive isotopically-shifted ^{31}P chemical shifts (ESI), free $H_xD_{3-x}B{\cdot}NMe_3$ – as shown by a loss of resolvable coupling in the ^{11}B NMR spectrum – and dissolved H_2/HD and D_2. This H/D exchange likely involves reversible oxidative cleavage of B–H or D_2 at the Rh(I)-centre followed by H/D exchange – *via* a σ-complex assisted metathesis (σ-CAM) mechanism.[54] Similar H/D exchange has been noted in related Rh-dihydrogen pincer complexes.[39,55]

The reaction between **1** and one equivalent of $H_3B{\cdot}NMe_2H$ initially follows the same course as with $H_3B{\cdot}NMe_3$ (Scheme 5). On time of mixing the complex [Rh(PONOP)(η^1-$H_3B{\cdot}NMe_2H$)][BAr^F_4], **3**, is observed to be the major organometallic product (greater than 95%), as identified by ^1H [δ −1.98, 3 H], ^{11}B [δ −21.3] and $^{31}P\{^1H\}$ [δ 212.9, J(RhP) = 138 Hz] NMR spectroscopies in comparison with complex **2**. The remainder is complex **1**. A triplet observed in the ^{11}B NMR spectrum (~10%) at δ −0.36 [J(BH) 110 Hz] is identified as $H_2B(NMe_2)_2H$,[56] and not boronium $[H_2B(NMe_2H)_2][BAr^F_4]$ by comparison with an independently prepared sample of the latter in $1,2\text{-}F_2C_6H_4$ (δ −2.15, J(BH) 117 Hz).[28] After 5 minutes aminoborane $H_2B{=}NMe_2$ [δ 37.8, t, J(BH) = 129 Hz][43,57] is observed, indicating dehydrogenation is proceeding that then eventually forms dimeric $[H_2BNMe_2]_2$ [δ 5.7, J(BH) = 127 Hz]. After 35 minutes this solution has changed to return **1** as the sole organometallic complex, during which time the $H_3B{\cdot}NMe_2H$ has undergone dehydrocoupling to form $[H_2BNMe_2]_2$ as the major product. The diamino-borane $HB(NMe_2)_2$ is the other, minor (2%), product [δ 28.7, d, J(BH) 130 Hz]. This formally comes from a hetero-dehydrocoupling of NMe_2H and $H_3B{\cdot}NMe_2H$.[51,58]

Catalysis and catalyst speciation: induction periods, change in resting state and a neutral hydride

These stoichiometric reactions demonstrate σ-complex formation, B–H activation, and competitive H_2 binding, and thus set the scene for the catalytic studies on $H_3B{\cdot}NMe_2H$ dehydrocoupling. Initial studies using catalyst **1** in a sealed NMR tube [2 mol%, $H_3B{\cdot}NMe_2H$ 0.144 M, 298 K, $1,2\text{-}F_2C_6H_4$ solution] revealed, by ^{11}B NMR spectroscopy (Fig. 2A), an induction period of approximately 300 seconds, followed by the consumption of $H_3B{\cdot}NMe_2H$ to finally give $[H_2BNMe_2]_2$ after 2700 s. $H_2B{=}NMe_2$ is observed to grow in and decay, with a

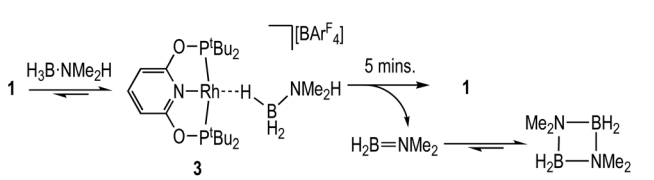

Scheme 5 Dehydrogenation of $H_3B{\cdot}NMe_2H$ by complex **1**.

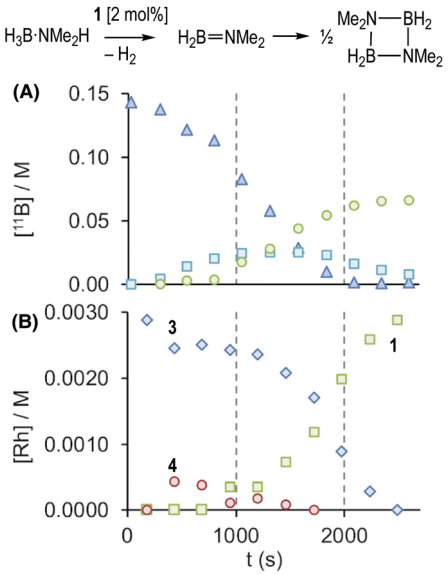

Fig. 2 Time course plots for dehydrogenation of $H_3B{\cdot}NMe_2H$ [0.144 M, 298 K, 1,2-$F_2C_6H_4$ solvent] using complex **1** (2 mol%) as measured by *in situ* NMR spectroscopy in a sealed NMR tube. (**A**) ^{11}B: △, $H_3B{\cdot}NMe_2H$; ○, $[H_2BNMe_2]_2$; □, $H_2B{=}NMe_2$. (**B**) $^{31}P\{^1H\}$: ◊, **3**; ○, **4**; □, **1**. Dotted lines to guide the eye.

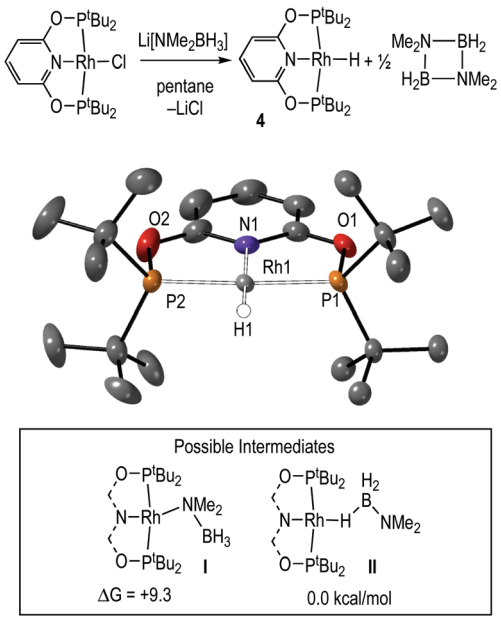

Fig. 3 Independent synthesis, solid-state structure of complex **4**, and possible intermediates. Displacement ellipsoids shown at the 30% level. Most H-atoms are not shown for clarity. Selected bond distances (Å) and angles (°): Rh1–H1, 1.54(5); Rh1–P1, 2.2179(17); Rh1–P2, 2.2020(17); Rh1–N1, 2.046(6); P1–Rh1–P2, 162.80(7). Free energies are DFT-calculated.

temporal profile characteristic of an intermediate. Following the same reaction by interleaved $^{31}P\{^1H\}$ NMR spectroscopy (Fig. 2B) revealed the immediate formation of the σ-amine-borane complex **3**, which reforms complex **1** as $H_3B{\cdot}NMe_2H$ is consumed and H_2 builds up in the reaction head-space. A further complex is observed to grow in and then out again, which is characterised by a $^{31}P\{^1H\}$ resonance at δ 225.4 [J(RhP) = 170 Hz] and a broad, high field, signal in the ^1H NMR spectrum at δ −10.13. This is identified by an independent synthesis as Rh(PONOP)H, **4**. Notably, **4** appears at the early stages of reaction, post-induction period, and is then consumed as **1** grows in. A small amount (~2%) of $HB(NMe_2)_2$ was also noted.

Complex **4**, Rh(PONOP)H, was independently synthesised by addition of the lithium amidoborane $Li[NMe_2BH_3]$[59] to Rh(PONOP)Cl in pentane solution, and is formed alongside $[H_2BNMe_2]_2$. Filtration and recrystallisation from methylcyclohexane afforded **4** as red crystals. Fig. 3 shows the solid-state structure of complex **4**, which was refined successfully as a two-component twin. The structural solution shows a pseudo square-planar coordination geometry around Rh in which the hydride ligand was located. The associated structural metrics are unremarkable, and complex **4** adds to the relatively small number of structurally characterised planar pincer monohydrides.[60–67] In the ^1H NMR spectrum of the isolated product (C_6D_6), the hydride ligand is signalled by a doublet of triplets at δ −9.60 [J(RhH) = 19.5, J(PH) = 22.6 Hz] that collapses into a doublet in the $^1H\{^{31}P\}$ NMR spectrum. In the $^{31}P\{^1H\}$ NMR spectrum a doublet is observed at δ 226.2 [J(RhP) = 171 Hz]. While these data are very similar to those observed during catalysis in 1,2-$F_2C_6H_4$ solution, the hydride chemical shift is different for pure material compared to that observed *in situ* during catalysis in this solvent: δ −9.92 and δ −10.13 respectively. This suggests the possibility of secondary, [Rh]–H···H–X, interactions[68] that are discussed in the computational section.

The mechanism to form **4** from Rh(PONOP)Cl could operate *via* an amidoborane[69–71] intermediate **I** (inset, Fig. 3) that undergoes β-elimination to generate **4** and $H_2B{=}NMe_2$ (experimentally observed as the dimer). Arguing against this is that β-elimination processes in group-2 amidoboranes have been found to be rather high in energy,[72] while the *ethyl* analogues M(PONOP)(CH_2CH_3) (M = Rh and Ir) have been reported to be unusually stable with regard to β-elimination and formation of the corresponding hydride.[73,74] An alternative mechanism is that $Li[NMe_2BH_3]$ acts as a simple hydride source,[75,76] avoiding **I** and directly eliminating LiCl and $H_2B{=}NMe_2$. DFT calculations suggest the latter scenario is more likely, with the σ-amidoborane adduct, Rh(PONOP)(H_3BNMe_2), **II**, computed to be 9.3 kcal mol^{-1} more stable than its N-bound isomer, Rh(PONOP)(NMe_2BH_3), **I**. Moreover, **II** exhibits a minimal barrier of 1.1 kcal mol^{-1} to B–H bond cleavage to form **4** and free H_2BNMe_2 (see ESI‡).

The role of boronium, $[NMe_2H_2][BAr^F{}_4]$, NMe_2H and the neutral hydride in catalytic turnover

With the identity of the intermediate complex **4** determined as being a neutral hydride, we considered possible routes for its formation and consumption in the catalytic ensemble, taking into account the induction period that is observed, that also precedes significant productive turnover. We have recently

reported[11] that for cationic [Rh(DPEphos)]$^+$-based dehydropolymerisation catalysts significant induction periods can be removed by adding amine, *e.g.* $NMeH_2$, as this promotes the formation of the active catalyst. While the actual mechanism of the active catalyst being brought on cycle with the [Rh(DPEphos)]$^+$-based catalysts is complex, one role of free amine (formed from B–N bond cleavage) is proposed to be attack at a cationic **σ**-amine-borane complex to afford a neutral hydride and boronium cation, *e.g.* $[H_2B(NMe_2H)_2]^+$.[28,31] The role of boronium in productive turnover has also been probed in pincer-like [Rh(Xantphos-^{i}Pr)]$^+$ systems, **B**,[30] and Pt-based systems related to **E**,[28] Scheme 2, as well as others.[29] We propose a similar set of fundamental processes operates here, in which amine-induced B–H bond cleavage gives a metal hydride that is then reprotonated. Two realistic scenarios presented themselves for this process: (a) the boronium route as described, or, (b) one that invoked the formation of ammonium (Scheme 6). This latter route is a deprotonation of σ-bound $H_3B{\cdot}NMe_2H$ to form an amidoborane, *i.e.* **II** Fig. 3, that then eliminates $H_2B{=}NMe_2$. Experiments to probe these and other fundamental steps in catalysis are detailed below, and also explored in the computational section.

(i) H_2 evolution experiments (0.072 M $H_3B{\cdot}NMe_2H$, 2 mol% **1**, eudiometer, 298 K) confirm an induction period (~450 s) also operates in an open system, before significant hydrogen production starts (TON = 50, max. rate (ν_{max}) = 1.0×10^{-4} M s^{-1}), Fig. 4, which is followed by an deceleration in rate consistent with substrate depletion. $[H_2BNMe_2]_2$ is produced as the principal product (^{11}B NMR), alongside a small amount of $HB(NMe_2)_2$. Periodic sampling demonstrates a similar profile for catalyst speciation as observed in a sealed NMR tube. There was no significant change in profile when Hg or sub-stoichiometric PPh_3 (0.2 equivalents) was added – suggesting a homogeneous process.[77] The post induction period reaction profile could not be reconciled with a simple kinetic model.

(ii) The induction period using catalyst **1** is removed by addition of one equivalent of NMe_2H at the start of catalysis, that also promotes a slightly faster turnover (ν_{max} = 1.6×10^{-4} M s^{-1}), Fig. 4. Again, the temporal profile could not be reconciled with a simple kinetic model. Speciation experiments under these conditions (sealed NMR tube) indicate that **4** is now formed exclusively at the start of catalysis, with no **3** observed. The final resting state is **1**. Amine thus promotes catalysis and moves the initial resting state to neutral **4**.

(iii) Adding one equivalent of $[H_2B(NMe_2H)_2][BAr^F{}_4]$ to catalyst **1** results in a much more pronounced induction profile (~450 s), and once turnover starts catalysis is slightly faster (ν_{max} = 1.8×10^{-4} M s^{-1}), and decelerates slower. However, as boronium is also a source of free NMe_2H on protonation of **4**, we cannot discount that it is simply acts in this way to promote catalysis (*vide infra*).

(iv) Addition of one equivalent of $[NMe_2H_2][BAr^F{}_4]$ to catalyst **1** increases the induction period to ~1 hour, but once turnover starts it is comparable to NMe_2H and $[H_2B(NMe_2H)_2]^+$ doped systems (ν_{max} = 2.0×10^{-4} M s^{-1}).

(v) Complex **4** is a poor catalyst on its own (0.072 M H_3BNMe_2H, 2 mol% **1**, eudiometer, 298 K), promoting slow turnover with only 25% conversion observed after ~1 h (ν_{max} = 0.5×10^{-4} M s^{-1}).

(vi) When complex **4** is doped with one equivalent of $[NMe_2H_2][BAr^F{}_4]$ the induction period is removed and catalysis proceeds at a rate comparable to the NMe_2H doped system (ν_{max} = 1.6×10^{-4} M s^{-1}). Doping with one equivalent of $[H_2B(NMe_2H)_2][BAr^F{}_4]$ also removes the induction period, but turnover is slower (ν_{max} = 0.5×10^{-4} M s^{-1}).

(vii) Under stoichiometric conditions addition of $[H_2B(NMe_2H)_2][BAr^F{}_4]$ or $[NMe_2H_2][BAr^F{}_4]$ to **4** recovers **1**.[78]

These observations show the important role of NMe_2H in catalysis, and that complex **1** can be regenerated by protonation of complex **4**. However, the kinetic profiles are still complex, and in particular changes in induction periods on doping suggest off-cycle processes and more complex equilibria are operating, while the precise role of $[NMe_2H_2][BAr^F{}_4]$ and/or $[H_2B(NMe_2H)_2][BAr^F{}_4]$ remain unclear. These points are explored in more detail next.

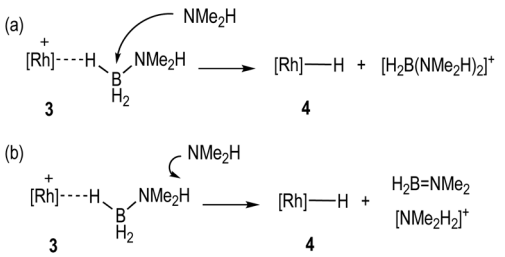

Scheme 6 Possible mechanisms for the formation of hydride **4**.

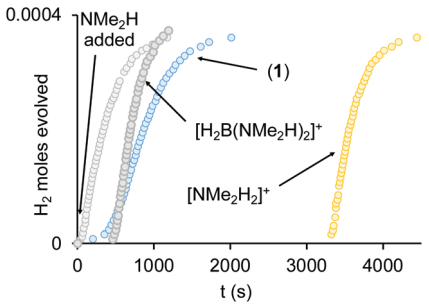

Fig. 4 Time course plot for dehydrogenation of $H_3B{\cdot}NMe_2H$ [0.072 M, 298 K, 1,2-$F_2C_6H_4$ solvent] using complex **1** (2 mol%), plus 1 equivalent NMe_2H, $[H_2B(NMe_2H)_2][BAr^F{}_4]$ or $[NMe_2H_2][BAr^F{}_4]$. H_2 as measured by H_2 eudiometer.

Kinetic analysis of H_2 generation

Given non-trivial temporal profiles we have deployed a combination of maximum rates[79] and Burés' graphical approach of Variable Time Normalisation Analysis (VTNA) to interrogate the kinetics of catalysis.[80,81] VTNA works by plotting reaction course (reactant or product) against $t[cat]^n$ for different $[cat]_{TOTAL}$. By adjusting the power value until the various plots visually overlay the order in $[cat]_{TOTAL}$ can be determined inde-

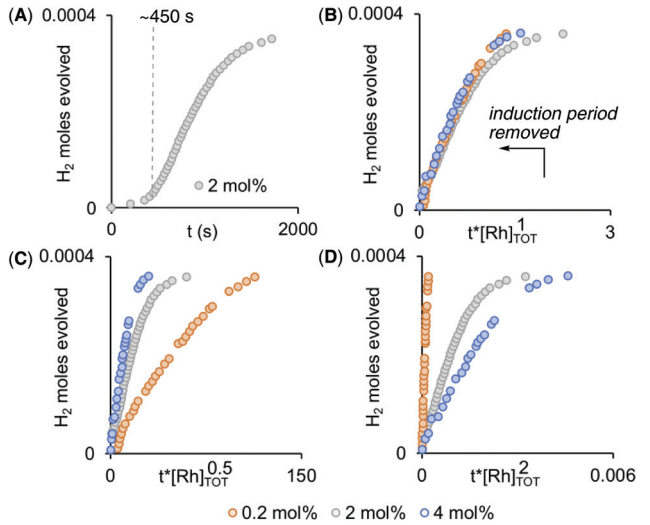

Fig. 5 (A) Time course plot for dehydrogenation of $H_3B{\cdot}NMe_2H$ [0.072 M, 298 K, 1,2-$F_2C_6H_4$ solvent] using complex **1** (2 mol%) as measured by H_2 evolution. Variable Time Normalization Analysis[80,81] for the order in $[Rh]_{TOT}$ (0.2 mol% – 4 mol%, induction periods removed): (**B**) $[Rh]^1$, (**C**) $[Rh]^{0.5}$, (**D**) $[Rh]^2$.

pendent of the complexity of the kinetic regime.[82] Fig. 5 shows this approach to determine the order in $[Rh]_{TOTAL}$, that demonstrates an overall first order kinetic regime between 0.2 mol% and 4 mol% $[Rh]_{TOTAL}$ – thus excluding any dimer/monomer equilibria in catalysis and also that $[Rh]_{TOTAL}$ remains approximately constant throughout. The data was time-shifted (~450 s) to remove the induction period that comes from the catalyst-independent B–N bond cleavage.

Given the complex kinetic profile, maximum rates (v_{max}) were used to determine the effect of isotopic substitution on the rate, and using $H_3B{\cdot}NMe_2D$ and $D_3B{\cdot}NMe_2H$ a k_H/k_D of 1.9 and 1.1 for NH and BH respectively was measured. This suggests that NH activation is involved in the rate-determining transition state, while BH activation is not.

The order in $H_3B{\cdot}NMe_2H$ was probed by determining the maximum rate measured as $[H_3B{\cdot}NMe_2H]$ was varied, while keeping $[Rh]_{TOTAL}$ fixed. Fig. 6 shows that this offers a profile that is initially positive order in amine-borane, but at higher concentrations of $H_3B{\cdot}NMe_2H$ the rate decelerates. This suggests that $H_3B{\cdot}NMe_2H$ is participating in an equilibrium that removes at least one of the reaction partners implicated

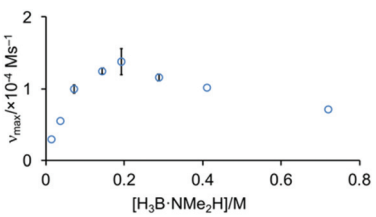

Fig. 6 Maximum rate of catalysis *versus* $[H_3B{\cdot}NMe_2H]$ using complex **1** (0.00144 M) as measured by H_2 evolution.

in, or prior to, the turn-over limiting step. A scenario that explains these data is an off-cycle interaction between $H_3B{\cdot}NMe_2H$ and $[H_2B(NMe_2H)_2]^+$ or $[NMe_2H_2]^+$ that would reduce the available concentration of $H_3B{\cdot}NMe_2H$ and $[H_2B(NMe_2H)_2]^+$ or $[NMe_2H_2]^+$; and depending on the relative concentrations could act in an inhibitory manner. We discount a scenario where the product (*i.e.* $[H_2BNMe_2]_2$) modifies the kinetics, as doping catalysis using **1** (2 mol%) with 50 equivalents of $[H_2BNMe_2]_2$ leads to no change in the temporal profile ($v_{max} = 1.0 \times 10^{-4}$ M s^{-1}).

Interaction between amine-boranes and $[H_2B(NMe_2H)_2][BAr^F{}_4]$ or $[NMe_2H_2][BAr^F{}_4]$: competing off-cycle equilibria

To probe the existence of off-cycle interactions, NMR titration experiments were carried out between $[H_2B(NMe_2H)_2][BAr^F{}_4]$ and $H_3B{\cdot}NMe_3$ or $H_3B{\cdot}NMe_2H$. Monitoring the change in the chemical shift of the NH protons in $[H_2B(NMe_2H)_2]^+$ as a function of amine-borane concentration generated titration isotherms. WinEQNMR2[83] analysis of the $H_3B{\cdot}NMe_3$ titration data determined a 1 : 1 stoichiometric association constant (K_a = 9.3(1) M^{-1}), Fig. 7A. We suggest adducts such as **III** with non-classical dihydrogen bonds are formed.[85] Related bisphosphine boronium adducts have been reported which show P–H···X hydrogen bonds.[84] For $H_3B{\cdot}NMe_2H$ the situation is more complex. Although the titration data clearly demonstrate an interaction between the two species, 1 : 1, 2 : 1 or 1 : 2 binding models failed to provide satisfactory agreement with experimental data, implying higher stoichiometry and/or complex equilibria. Nevertheless, these experiments show that $H_3B{\cdot}NMe_2H$ and $[H_2B(NMe_2H)_2][BAr^F{}_4]$ can form off-cycle adducts that attenuate the availability of both. Similar 1 : 1 equilibria are also operating with $[NMe_2H_2][BAr^F{}_4]/H_3B{\cdot}NMe_3$, K_a = 28(2) M^{-1}, possibly *via* adducts such as **IV**, Fig. 7B. At high $[H_3B{\cdot}NMe_2H]$ the decrease in max rate suggests these interactions (with whichever partner) are significant enough to cause a relative reduction in rate. Similar adducts could also be involved in sequestering free amine-leading to the change

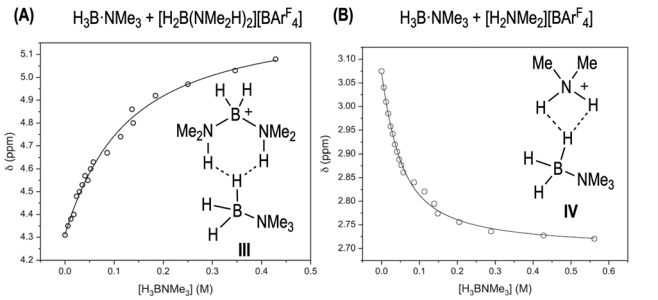

Fig. 7 (A) Titration binding curve of $[H_2B(NMe_2H)_2][BAr^F{}_4]$ (298 K, 30 mM, 1,2-$F_2C_6H_4$) with $H_3B{\cdot}NMe_3$. Fitted binding isotherm is indicated by line. Association Constant, K_a, 9.3(1) M^{-1}, calculated using WinEQNMR2[83] monitoring the chemical shift data for the NH protons in $[H_2B(NMe_2H)_2][BAr^F{}_4]$. (B) Titration binding curve of $[NMe_2H_2][BAr^F{}_4]$ (298 K, 30 mM, 1,2-$F_2C_6H_4$) with $H_3B{\cdot}NMe_3$. Association Constant, K_a, 28 (2) M^{-1} derived from monitoring the chemical shift data for the NMe protons in $H_3B{\cdot}NMe_3$.

in induction periods observed when $[H_2B(NMe_2H)_2][BAr^F{}_4]$ or $[NMe_2H_2][BAr^F{}_4]$ are doped into catalysis; and productive turnover only occurs once sufficient NMe_2H has been formed by B–N bond cleavage to overcome these off-cycle equilibria. Crystallographically characterized $[R_2NH_2\cdots NR_2H]^+$ complexes are known.[86]

Elementary steps of the mechanism

Pulling these observations together a catalytic cycle can be proposed, Scheme 7. ①: σ-Dihydrogen complex **1** reversibly reacts with $H_3B{\cdot}NMe_2H$ to form **3**, that is observed to be the major species at the very start of catalysis. ②: NMe_2H (formed from slow B–N bond cleavage of $H_3B{\cdot}NMe_2H$) then rapidly reacts with **3** to form **4**, and either $[H_2B(NMe_2H)_2]^+$ or $[NMe_2H_2]^+$/$H_2B{=}NMe_2$. ③: Protonation of **4** regenerates **1**, free $NMeH_2$ and in the case of boronium, $H_2B{=}NMe_2$ that dimerises to give $[H_2BNMe_2]_2$. The concentration of **1**/**4**/**3** follows temporal profiles (Fig. 2) that suggest they are closely matched in relative stabilities and their concentrations thus depend on how $[H_3B{\cdot}NMe_2H]$ and $[H_2]$ evolve throughout catalysis. Off-cycle equilibria between $H_3B{\cdot}NMe_2H$ and either $[H_2B(NMe_2H)_2]^+$ or $[NMe_2H_2]^+$ operate to modify the available concentration of species involved in turnover. The measured KIE indicates NH activation is involved in the turnover limiting transition state. This could come from step ② being turnover limiting in the ammonium pathway (N–H cleavage of $H_3B{\cdot}NMe_2H$), or step ③ in both boronium or ammonium pathways (N–H cleavage to reprotonate **4**). The lack of a significant KIE measured for BH argues that B–H bond cleavage is not significant in the turnover limiting transition state. As the experimental data do not allow for discrimination between an ammonium or a boronium pathway we turned to computational studies to determine the relative energies of each pathway.

Computational studies

The details of the dehydrogenation and protonation steps (**3** → **4** → **1**) were also probed with DFT calculations. The model used incorporated the full PONOP ligand with geometries optimised with the BP86 functional. Free energies were then corrected for solvation, dispersion (BJD3) and basis set effects (def2TZVP, see ESI‡ for full details). 2-Hexanone (ε = 14.14) was employed as solvent as a model for 1,2-difluorobenzene (ε = 13.81) for which parameters are not currently available. Two pathways were considered for $H_3B{\cdot}NMe_2H$ dehydrogenation from **3** and free NMe_2H to form **1** (see Scheme 8): initial nucleophilic attack at B to form boronium (following the proposal of Conejero and co-workers[28]) and N–H deprotonation of the bound $H_3B{\cdot}NMe_2H$ ligand, *i.e.* the ammonium route.[87] Both processes initially form **4** which is then reprotonated by either $[H_2B(NMe_2H)_2]^+$ or $[NMe_2H_2]^+$ to form **1**. Alternative processes based on B–H and/or N–H activation from **3** without amine or boronium involvement were also considered and shown to be significantly higher in energy (see Fig. S1–S3, ESI‡).

Starting from **3** (Scheme 8 centre), a H-bonded adduct, $\mathbf{3}{\cdot}NMe_2H$ (+2.8 kcal mol^{-1}), is formed that features a short NH···N distance of 1.76 Å. Nucleophilic attack at B then passes through $\mathbf{TS(3\text{-}4)_B}$ at +24.9 kcal mol^{-1} to form $\mathbf{4}{\cdot}HMe_2NBH_2NMe_2H^+$ with a strong Rh–$H^{\delta-}\cdots H^{\delta+}$–N dihydrogen interaction (1.75 Å). This is thus set up for facile proton transfer *via* $\mathbf{TS(4\text{-}1)_B}$ (+10.1 kcal mol^{-1}) to give $[(PONOP)Rh(\eta^2\text{-}H_2)]^+$, **1**, initially as an H-bonded adduct with the $Me_2NBH_2NMe_2H$ moiety. Release of H_2BNMe_2 and NMe_2H along with substitution of H_2 in **1** by $H_3B{\cdot}NMe_2H$ (see Scheme 9) then reforms **3** and completes the catalytic cycle. The overall process is exergonic by 5.6 kcal mol^{-1} and has an energy span of 24.9 kcal mol^{-1}. The alternative N–H deprotonation of the $H_3B{\cdot}NMe_2H$ ligand in $\mathbf{3}{\cdot}NMe_2H$ proceeds through $\mathbf{TS(3\text{-}4)_N}$ at +17.9 kcal mol^{-1} and occurs with concomitant B–H bond cleavage to give neutral hydride **4**, as a weakly bound adduct with H_2BNMe_2 and $[H_2NMe_2]^+$. Removal of H_2BNMe_2 allows formation of $\mathbf{4}{\cdot}H_2NMe_2^+$ (−1.7 kcal mol^{-1}). This again features a strong Rh–$H^{\delta-}\cdots H^{\delta+}$–N interaction (1.55 Å) and allows proton transfer to give $\mathbf{1}{\cdot}NMe_2H$ at +6.8 kcal mol^{-1}. Loss of NMe_2H and $H_2/H_3B{\cdot}NMe_2H$ substitution again completes the cycle. The overall barrier for this *N*-deprotonation mechanism is 17.9 kcal mol^{-1} and is therefore predicted to be favoured over nucleophilic attack at B.

Scheme 9 shows the details of the $H_2/H_3B{\cdot}NMe_2H$ substitution to reform **3** from **1**. An associative transition state could not be located, but instead initial, very facile oxidative cleavage of the η^2-H_2 ligand permits formation of an η^1-$H_3B{\cdot}NMe_2H$ Rh(III) adduct, $\mathbf{Int(1\text{-}3)2}$, at +5.6 kcal mol^{-1}. Reductive elimination of H_2 then proceeds *via* $\mathbf{TS(1\text{-}3)3}$ at +15.3 kcal mol^{-1} to form **3**.[88]

Returning to Scheme 8, the computed geometries of the key transition states show $\mathbf{TS(3\text{-}4)_B}$ is similar to that located by Conejero and co-workers in their study,[28] and features significant B–H stretching corresponding to hydride transfer onto the Rh centre. In contrast $\mathbf{TS(3\text{-}4)_N}$ exhibits a much later geometry in which hydride transfer to Rh is complete and significant H^+ transfer to form the $[H_2NMe_2]^+$ cation is evident. As a result $\mathbf{TS(3\text{-}4)_N}$ displays a very large dipole moment (24.7 D) making its energy sensitive to solvation effects.[89] $\mathbf{TS(3\text{-}4)_N}$ is favoured on energetic grounds and would be expected to show a small N–H/N–D KIE (and no B–H/B–D KIE). In contrast the

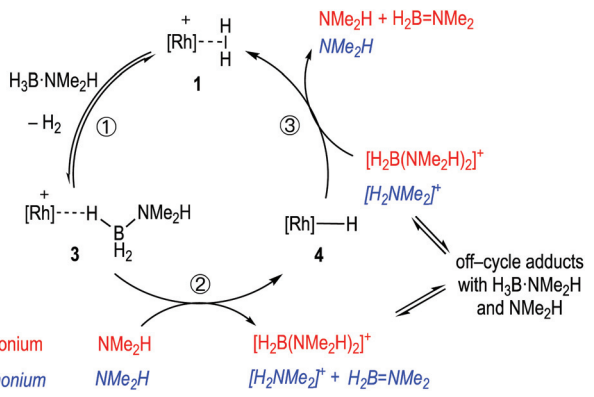

Scheme 7 Suggested simplified catalytic cycle with boronium (red) ammonium (blue, italics) and pathways.

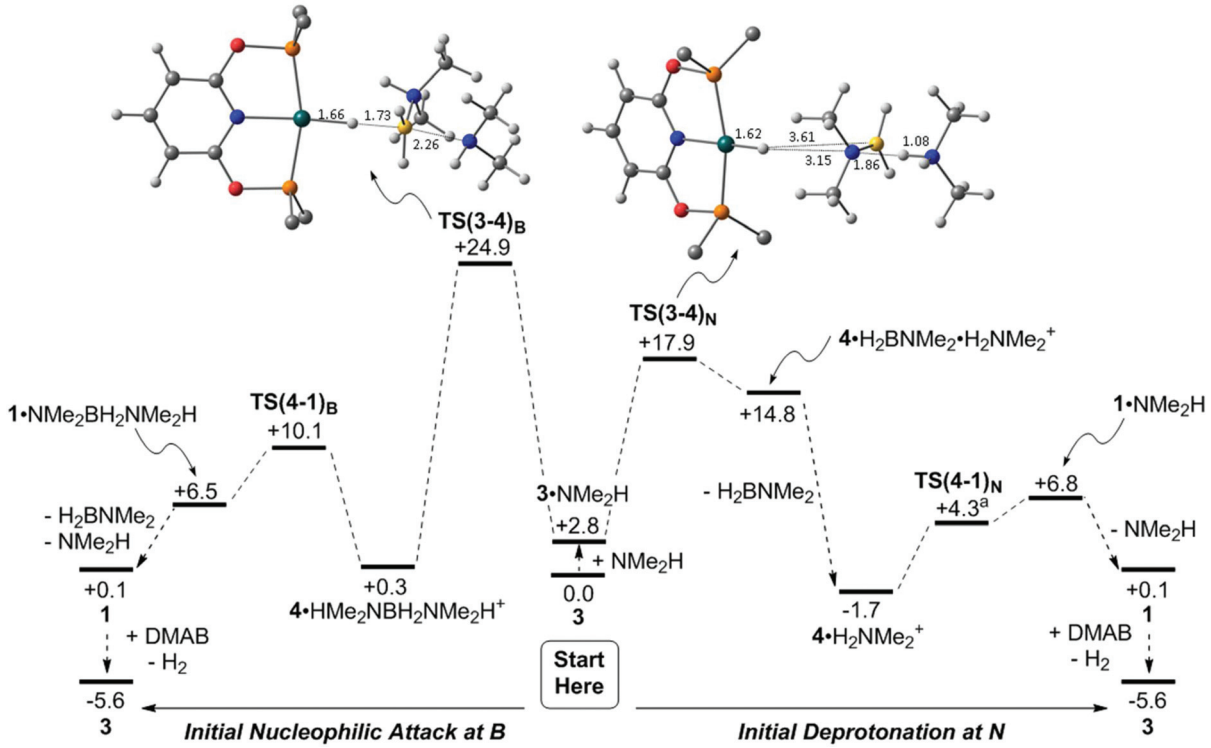

Scheme 8 Computed free energy profiles (kcal mol^{-1}) for dehydrogenation of $H_3B{\cdot}NMe_2H$ from H-bonded adduct **3** (centre) *via* initial nucleophilic attack at B (left) or initial deprotonation at N (right). [Rh] = (PONOP)Rh. Energies are quoted relative to **3** + free $H_3B{\cdot}NMe_2H$ and NMe_2H set to 0.0 kcal mol^{-1}. Ball and stick representations of $\mathbf{TS(3\text{-}4)_B}$ and $\mathbf{TS(3\text{-}4)_N}$ have the *t*Bu Me groups removed for clarity and all distances are given in Å. Atom colouring scheme: Rh (teal); C (grey); H (while); O (red); N (blue); P (orange); B (yellow). [a] $\mathbf{TS(4\text{-}1)_N}$ is a true stationary point on the electronic energy surface but differential zero-point energy effects cause the free energy of this species to fall below $\mathbf{1}{\cdot}NMe_2H$.

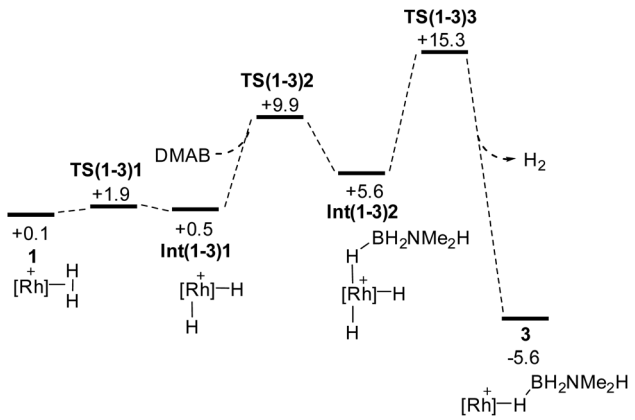

Scheme 9 Computed free energy profiles (kcal mol^{-1}) for H_2/$H_3B{\cdot}NMe_2H$ substitution in **1** to reform **3**; $[Rh]^+$ = $[Rh(PONOP)]^+$. Energies are quoted relative to **3** + free $H_3B{\cdot}NMe_2H$ and NMe_2H set to 0.0 kcal mol^{-1}.

significant B–H bond stretching in $\mathbf{TS(3\text{-}4)_B}$ would imply a significant B–H/B–D KIE that is not seen experimentally.

The computed energies of **1**, **3** and **4** in Scheme 8 bear comparison with the time course plots derived from experiment in Fig. 2. **1** and **3** are computed to be most stable as isolated species, however **4** is present as the dihydrogen-bonded adduct $\mathbf{4}{\cdot}H_2NMe_2^+$. This formulation is also consistent with the small shift in ^1H chemical shift associated with this species under catalytic conditions. Overall these three species are all within 1.8 kcal mol^{-1} of each other. The barriers for the formation of **4** (as $\mathbf{4}{\cdot}H_2NMe_2^+$, $\Delta G^{\ddagger}$ = 17.9 kcal mol^{-1} *via* $\mathbf{TS(3\text{-}4)_N}$) and its onward reaction to reform **3** ($\Delta G^{\ddagger}$ = 17.0 kcal mol^{-1}, *i.e.* from $\mathbf{4}{\cdot}H_2NMe_2^+$ at −1.7 kcal mol^{-1} to $\mathbf{TS(1\text{-}3)3}$ at +15.3 kcal mol^{-1}) are also finely balanced. The computed energetics therefore reflect the observation of **1**, **3** and **4** during catalysis.

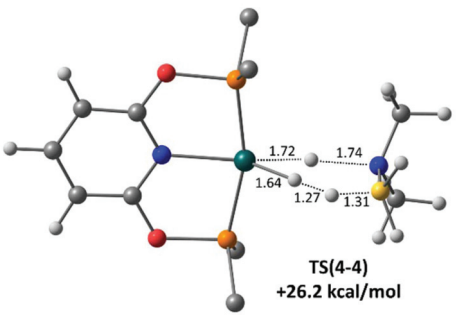

Fig. 8 Computed geometry of **TS(4-4)** for dehydrogenation of $H_3B{\cdot}NMe_2H$ at **4**, with selected distances in Å. Energies is quoted relative to **4** + free $H_3B{\cdot}NMe_2H$ set to 0.0 kcal mol^{-1}. Rh (teal); C (grey); H (while); O (red); N (blue); P (orange); B (yellow).

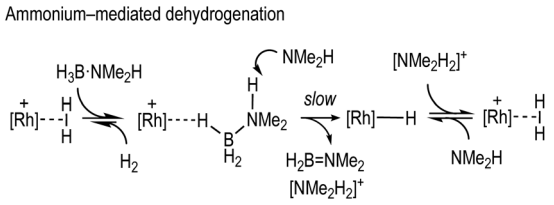

Scheme 10 Hydride transfer and reprotonation *via* ammonium.

Finally, $H_3B{\cdot}NMe_2H$ dehydrogenation at the neutral hydride **4** was also assessed and a novel concerted transition state, **TS (4-4)**, involving B–H transfer onto the Rh–H ligand, with concomitant N–H transfer onto the Rh centre was characterised (Fig. 8). This releases not only H_2BNMe_2 but also H_2 in a single step, regenerating **4** with a computed barrier of 26.2 kcal mol^{-1}. This barrier is significantly higher than that for the amine-assisted pathway in Scheme 8 and so is consistent with the poor performance of isolated **4** as a dehydrocoupling catalyst.[90] We have recently reported a similar amine-borane dehydrogenation transition state at an Fe–H species.[91]

Conclusions

By using the $[Rh(PONOP)(\eta^2\text{-}H_2)][BAr^F{}_4]$ precatalyst, which has a labile dihydrogen ligand, we have been able to map out the catalytic dehydrocoupling of $H_3B{\cdot}NMe_2H$ using a pincer complex. As is becoming increasingly apparent,[28,30,31] for cationic systems a hydride transfer/reprotonation route from a σ-bound amine-borane is a viable pathway for dehydrogenation when using cationic catalysts. While this can occur *via* a nucleophilic attack on B, *via* a boronium (*i.e.* Scheme 2), we show here that an alternative pathway of deprotonation of the σ-bound amine-borane to form an intermediate ammonium salt is also a viable route (Scheme 10). Central to both these processes is the generation of free amine from B–N bond cleavage to act as a nucleophile or base respectively. We,[11] and others,[24] have recently commented on the role of amine in promoting catalytic turnover in a variety of dehydrocoupling systems; and there is a very recent complementary report of the stoichiometric role of ammonium/amine in the protonation of borohydride complexes to eventually form σ-bound aminoboranes.[92] In the system under discussion here the amine-assisted formation of the neutral hydride, *i.e.* **4**, and $[NMe_2H_2]^+$ is rate limiting in catalysis, although this may not necessarily be the case for every system in a more general sense. Whatever the precise barriers of each step, the off-cycle equilibria involving $[NMe_2H_2]^+$ (or $[H_2B(NMe_2H)_2]^+$ in a boronium route) will likely have an additional influence on the overall kinetics. A more detailed understanding of the role of initial B–N bond cleavage, to form free amine and the resulting co-catalysts, in dehydrocoupling – and especially dehydropolymerisation – could well be important in building an overarching general mechanism for such processes.

Experimental

All manipulations, unless otherwise stated, were performed under an argon atmosphere using standard Schlenk line and glovebox techniques. Glassware was oven dried at 130 °C overnight and flame dried under vacuum prior to use. Pentane, hexane, toluene, Et_2O and CH_2Cl_2 were dried using a Grubbs-type solvent purification system (MBraun SPS-800) and degassed by three successive freeze–pump–thaw cycles.[93] THF was dried over Na/benzophenone, vacuum distilled, degassed by three successive freeze–pump–thaw cycles and stored over 3.0 Å molecular sieves. 1,2-$F_2C_6H_4$ (pre-treated with alumina) and CD_2Cl_2 were dried over CaH_2, vacuum distilled, degassed by three successive freeze–pump–thaw cycles and stored over 3.0 Å molecular sieves. $H_3B{\cdot}NMe_3$ and $H_3B{\cdot}NMe_2H$ were purchased from Sigma-Aldrich and sublimed prior to use (5.0×10^{-2} mbar, 298 K and 303 K respectively). Hg (99.9995%) was purchased from Sigma-Aldrich, washed with 1,2-$F_2C_6H_4$ and dried *in vacuo* prior to use. PPh_3 and *n*-butyllithium (2.5 M in hexanes) were purchased from Sigma-Aldrich and used as received. $BH_3{\cdot}THF$ (1.0 M in THF) and NMe_2H (2.0 M in THF) were purchased from Fisher Scientific and used as received to form solutions in 1,2-$F_2C_6H_4$ of the desired concentrations. $Na[BAr^F{}_4]$ (Ar^F = 3,5-$(CF_3)_2C_6H_3$),[46] $[BH_2(NMe_2H)_2][BAr^F{}_4]$,[28,94] $D_3B{\cdot}NMe_3$,[95] $H_3B{\cdot}NMe_2D$,[96] Rh(PONOP)C[47] and **1**[39,97] were prepared by literature methods.

NMR spectra were recorded on a Bruker AVIIIHD 500 or Bruker AVIIIHD 400 nanobay spectrometer at room temperature, unless otherwise stated. Residual protio solvent was used as a reference for ^1H NMR spectra in deuterated solvent samples. For 1,2-$F_2C_6H_4$ solvent the NMR spectrometer was pre-locked to a sample of C_6D_6 (25%) and 1,2-$F_2C_6H_4$ (75%) and referenced to the centre of the downfield solvent multiplet, δ = 7.07. ^{31}P and ^{11}B NMR spectra were referenced externally against 85% H_3PO_4 and $BF_3{\cdot}OEt_2$ respectively. Chemical shifts (δ) are quoted in ppm and coupling constants (J) in Hz. Electrospray ionization mass spectrometry (ESI-MS) of organometallic complexes were recorded using a Bruker MicrOTOF instrument directly connected to a modified Innovative Technology glovebox.[98] Samples were diluted in 1,2-$F_2C_6H_4$ to a concentration of approximately 1.0×10^{-6} M before analysis. Elemental microanalyses were performed by Stephen Boyer at London Metropolitan University.

Synthesis of $[Rh(PONOP)(H_3B{\cdot}NMe_3)][BAr^F{}_4]$ (2)

1 (50 mg, 0.036 mmol) and $H_3B{\cdot}NMe_3$ (2.62 mg, 0.036 mmol) were dissolved in 1,2-$F_2C_6H_4$ (2 mL) and the reaction stirred at room temperature for 24 h. The solution was then concentrated *in vacuo* to *ca.* 1 mL, cooled to 0 °C and pentane (5 mL) was added to give a precipitate. The solid was isolated by filtration and washed with pentane (2 mL × 2) before being dried under vacuum to give the product as a yellow powder. An isolated yield 32.8 mg (63%) was obtained. Layering a 1,2-$F_2C_6H_4$ solution of complex **2** with pentane and storing at 5 °C overnight yielded dark yellow crystals suitable for single crystal X-ray diffraction.

^{1}H NMR (500 MHz, CD_2Cl_2, 298 K). δ 7.73 (br s, 8H, [BAr^F_4]-*o*-CH), 7.69 (obscured tr, $^3J_{HH}$ 8.0, 1H, C_5H_3N), 7.56 (br s, 4H, [BAr^F_4]-*p*-CH), 6.67 (d, $^3J_{HH}$ 8.0, 2H, C_5H_3N), 2.72 (s, 9H, NMe_3), 1.42 (vt, J_{PH} 8.0, 36H, P(^{t}Bu)$_2$), −2.55 (br d, 3H, RhH_3B).

^{11}B NMR (160 MHz, CD_2Cl_2, 298 K). δ −6.61 (s, [BAr^F_4]), −15.24 (br s, RhH_3B).

^{31}P{^{1}H} NMR (202 MHz, CD_2Cl_2, 298 K). δ 208.9 (d, $^1J_{RhP}$ 141.6).

ESI-MS (1,2-$F_2C_6H_4$, 60 °C, 4.5 kV). *m*/*z* 575.26 (calc. 575.26 for [Rh(PONOP)($H_3B{\cdot}NMe_3$)]$^+$ fragment).

Elemental microanalysis. Calc. $C_{56}H_{63}B_2F_{24}N_2O_2P_2Rh$ (1438.57 gmol^{-1}) C, 46.76; H, 4.41; N, 1.95. Found: C, 46.90; H, 4.27; N, 2.01.

Spectroscopic data for [Rh(PONOP)($H_3B{\cdot}NMe_2H$)][BAr^F_4] (3)

^{1}H NMR (500 MHz, 1,2-$F_2C_6H_4$, 298 K). δ 8.32 (br s, 8H, [BAr^F_4]-*o*-CH), 7.69 (br s, 4H, [BAr^F_4]-*p*-CH), 7.61 (tr, $^3J_{HH}$ 8.0, 1H, C_5H_3N), 6.67 (d, $^3J_{HH}$ 8.3, 2H, C_5H_3N), 3.25 (br s, 1H, NH), 2.76 (d, *J* 5.6, 6H, NMe_2), 1.42 (vt, J_{PH} 7.4, 36H, P(*t*Bu)$_2$), −1.98 (br d, 3H, RhH_3B).

^{11}B NMR (160 MHz, 1,2-$F_2C_6H_4$, 298 K). δ −6.22 (s, [BAr^F_4]), −21.36 (br s, RhH_3B).

^{31}P{^{1}H} NMR (202 MHz, 1,2-$F_2C_6H_4$, 298 K). δ 212.9 (d, $^1J_{RhP}$ 137.5).

Synthesis of Li[$H_3B{\cdot}NMe_2$][59]

Hexane (20 mL) was added to $H_3B{\cdot}NMe_2H$ (400 mg, 6.79 mmol) to give a white suspension, which was then cooled to −78 °C. *n*-Butyllithium (2.5 M, 3 mL, 7.5 mmol) was added dropwise by syringe over 15 minutes. The reaction was stirred at −78 °C for 1 hour and then allowed to come to room temperature and stirred for an additional hour. The solution was then filtered, leaving a white solid which was washed with hexane. The solid was dried cold *in vacuo* for 2 hours to yield a white powder (412.9 mg, 94% yield).

^{11}B NMR (128 MHz, THF, 298 K). δ −14.45 (q, J_{BH} 86.9).

Synthesis of Rh(PONOP)H (4)

Rh(PONOP)Cl (150 mg, 0.279 mmol) and Li[$H_3B{\cdot}NMe_2$] (36.2 mg, 0.558 mmol) were dissolved in pentane (5 mL) to give an orange/red solution, which was stirred at room temperature for 24 hours. The solution was then filtered and the solvent removed *in vacuo* and dried under vacuum overnight to yield a red powder. An isolated yield of 113.3 mg (81% yield) was obtained. A concentrated solution of **4** in methylcyclohexane was stored at 5 °C for 1 hour and then moved to −20 °C and after 3 days, red crystals suitable for single crystal X-ray diffraction were formed.

^{1}H NMR (400 MHz, C_6D_6, 298 K). δ 6.92 (tr, $^3J_{HH}$ 8.0, 1H, C_5H_3N), 6.27 (d, $^3J_{HH}$ 7.9, 2H, C_5H_3N), 1.41 (vt, J_{PH} 6.9, 36H, P(*t*Bu)$_2$), −9.60 (td, J_{PH} 22.6, J_{RhH} 19.5, 1H, RhH).

^{1}H{^{31}P} NMR (400 MHz, C_6D_6, 298 K). δ 6.92 (tr, $^3J_{HH}$ 8.0, 1H, C_5H_3N), 6.28 (d, $^3J_{HH}$ 7.9, 2H, C_5H_3N), 1.42 (s, 36H, P(*t*Bu)$_2$), −9.60 (d, J_{RhH} 19.6, 1H, RhH).

^{31}P{^{1}H} NMR (162 MHz, C_6D_6, 298 K). δ 226.2 (d, $^1J_{RhP}$ 171.2).

^{13}C{^{1}H} NMR (100 MHz, C_6D_6, 298 K). δ 28.7 (vt, J_{CP} 5.3, 12C, P–C(CH_3)$_3$), 39.0 (vq, J_{CPRh} 3.9, 4C, P–C(CH_3)$_3$), 100.8 (d, J_{CP} 2.3, 2C, C_5H_3N), 135.9 (s, 1C, C_6H_5N), 163.4 (vt, J_{CP} 4.9, 2C, C_6H_5N).

Elemental microanalysis. Calc. $C_{21}H_{40}NO_2P_2Rh$ (503.41 gmol^{-1}) C, 50.10; H, 8.01; N, 2.78. Found: C, 49.99; H, 8.09; N, 2.86.

Synthesis of $D_3B{\cdot}NMe_2H$

$D_3B{\cdot}NMe_2H$ was prepared by a modification of the literature procedure for the synthesis of $D_3B{\cdot}NMeH_2$.[95] $D_3B{\cdot}NMe_3$ (200 mg, 2.6 mmol, 99% D) was added to a J. Young flask and cooled to −78 °C. NMe_2H (2.0 M in THF, 7 mL, 132.0 mmol) was added to the $D_3B{\cdot}NMe_3$, the solution allowed to warm to room temperature and was stirred for 72 hours. The volatiles were removed *in vacuo* at 0 °C and the resulting solid purified by sublimation (5.0×10^{-2} mbar, 303 K) to give a white solid (130 mg, 80% yield). NMR data as reported previously in the literature.[96]

General procedure for kinetic measurements of the catalytic dehydrogenation of $H_3B{\cdot}NMe_2H$

Under closed/NMR tube conditions. In a typical experiment (*e.g.* 2 mol% catalyst loading), $H_3B{\cdot}NMe_2H$ (3.4 mg, 57.7 μmol) was dissolved in 1,2-$F_2C_6H_4$ (0.4 mL) in a Schlenk flask and 0.2 mL of this solution was added to a J. Young's high-pressure NMR tube. In a separate flask, **1** (2 mg, 1.4 μmol) was dissolved in 1,2-$F_2C_6H_4$ (0.5 mL) and 0.2 mL of this solution was added to the same NMR tube, which was immediately sealed and then frozen in $N_{2(l)}$. When the NMR spectrometer was set up for kinetic measurements, the NMR tube was thawed, shaken thoroughly and immediately inserted into the NMR spectrometer for analysis.

Under hydrogen evolution measurement conditions. In typical experiment (*e.g.* 2 mol% catalyst loading), $H_3B{\cdot}NMe_2H$ (21.2 mg, 0.36 mmol) was dissolved in 1,2-$F_2C_6H_4$ (4 mL) in a jacketed two-neck Schlenk flask connected to a recirculating cooler and the temperature set to 25 °C. In a separate Schlenk flask, **1** (11.8 mg, 8.6 μmol) was dissolved in 1,2-$F_2C_6H_4$ (1.2 mL). The flask containing amine-borane was sealed off from the argon supply and connected to a water-filled 100.0 mL gas burette. 1 mL of the catalyst solution was added to the reaction mixture and the resultant solution was stirred at 400 rpm. The volume of gas evolved was then recorded as function of time, starting from the addition of catalyst to amine-borane.

Conflicts of interest

There are no conflicts of interest.

Acknowledgements

University of Oxford, Heriot-Watt University, the EPSRC (DTP and EP/M024210/1) and SCG Chemicals Co. Ltd for funding.

The ToC for this article was prepared using Catacycle.[99] David Ryan for stimulating and insightful discussions.

Notes and references

1 A. Staubitz, A. P. M. Robertson, M. E. Sloan and I. Manners, *Chem. Rev.*, 2010, **110**, 4023–4078.
2 R. Waterman, *Chem. Soc. Rev.*, 2013, **42**, 5629–5641.
3 H. C. Johnson, T. N. Hooper and A. S. Weller, *Top. Organomet. Chem.*, 2015, **49**, 153–220.
4 A. Rossin and M. Peruzzini, *Chem. Rev.*, 2016, **116**, 8848–8872.
5 S. Bhunya, T. Malakar, G. Ganguly and A. Paul, *ACS Catal.*, 2016, **6**, 7907–7934.
6 E. M. Leitao, T. Jurca and I. Manners, *Nat. Chem.*, 2013, **5**, 817–829.
7 A. Staubitz, A. Presa Soto and I. Manners, *Angew. Chem., Int. Ed.*, 2008, **47**, 6212–6215.
8 A. Staubitz, M. E. Sloan, A. P. M. Robertson, A. Friedrich, S. Schneider, P. J. Gates, J. Schmedt auf der Günne and I. Manners, *J. Am. Chem. Soc.*, 2010, **132**, 13332–13345.
9 D. Han, F. Anke, M. Trose and T. Beweries, *Coord. Chem. Rev.*, 2019, **380**, 260–286.
10 *Smart Inorganic Polymers: Synthesis, Properties, and Emerging Applications in Materials and Life Sciences*, ed. E. Hey-Hawkins and M. Hissler, Wiley-VCH, Weinheim, 2019.
11 G. M. Adams, D. E. Ryan, N. A. Beattie, A. I. McKay, G. C. Lloyd-Jones and A. S. Weller, *ACS Catal.*, 2019, **9**, 3657–3666.
12 V. Du, G. Whittell and I. Manners, *Dalton Trans.*, 2016, **45**, 1055–1062.
13 D. A. Resendiz-Lara, N. E. Stubbs, M. I. Arz, N. E. Pridmore, H. A. Sparkes and I. Manners, *Chem. Commun.*, 2017, **53**, 11701–11704.
14 X. Wang, T. N. Hooper, A. Kumar, I. K. Priest, Y. Sheng, T. O. M. Samuels, S. Wang, A. W. Robertson, M. Pacios, H. Bhaskaran, A. S. Weller and J. H. Warner, *CrystEngComm*, 2017, **19**, 285–294.
15 A. L. Colebatch and A. S. Weller, *Chem. – Eur. J.*, 2019, **25**, 1379–1390.
16 B. L. Dietrich, K. I. Goldberg, D. M. Heinekey, T. Autrey and J. C. Linehan, *Inorg. Chem.*, 2008, **47**, 8583–8585.
17 A. Kumar, H. C. Johnson, T. N. Hooper, A. S. Weller, A. G. Algarra and S. A. Macgregor, *Chem. Sci.*, 2014, **5**, 2546–2553.
18 M. Shimoi, S.-i. Nagai, M. Ichikawa, Y. Kawano, K. Katoh, M. Uruichi and H. Ogino, *J. Am. Chem. Soc.*, 1999, **121**, 11704–11712.
19 M. A. Esteruelas, A. M. López and M. Oliván, *Chem. Rev.*, 2016, **116**, 8770–8847.
20 A. Paul and C. B. Musgrave, *Angew. Chem., Int. Ed.*, 2007, **46**, 8153–8156.
21 E. M. Titova, E. S. Osipova, A. A. Pavlov, O. A. Filippov, S. V. Safronov, E. S. Shubina and N. V. Belkova, *ACS Catal.*, 2017, **7**, 2325–2333.
22 M. A. Esteruelas, P. Nolis, M. Oliván, E. Oñate, A. Vallribera and A. Vélez, *Inorg. Chem.*, 2016, **55**, 7176–7181.
23 A. N. Marziale, A. Friedrich, I. Klopsch, M. Drees, V. R. Celinski, J. Schmedt auf der Günne and S. Schneider, *J. Am. Chem. Soc.*, 2013, **135**, 13342–13355.
24 A. Glüer, M. Förster, V. R. Celinski, J. Schmedt auf der Günne, M. C. Holthausen and S. Schneider, *ACS Catal.*, 2015, **5**, 7214–7217.
25 X. Zhang, L. Kam, R. Trerise and T. J. Williams, *Acc. Chem. Res.*, 2017, **50**, 86–95.
26 P. Bhattacharya, J. A. Krause and H. Guan, *J. Am. Chem. Soc.*, 2014, **136**, 11153–11161.
27 W. E. Piers, S. C. Bourke and K. D. Conroy, *Angew. Chem., Int. Ed.*, 2005, **44**, 5016–5036.
28 M. Roselló-Merino, J. López-Serrano and S. Conejero, *J. Am. Chem. Soc.*, 2013, **135**, 10910–10913.
29 S. Pal, S. Kusumoto and K. Nozaki, *Organometallics*, 2018, **37**, 906–914.
30 G. M. Adams, A. L. Colebatch, J. T. Skornia, A. I. McKay, H. C. Johnson, G. C. Lloyd-Jones, S. A. Macgregor, N. A. Beattie and A. S. Weller, *J. Am. Chem. Soc.*, 2018, **140**, 1481–1495.
31 A. Kumar, N. A. Beattie, S. D. Pike, S. A. Macgregor and A. S. Weller, *Angew. Chem., Int. Ed.*, 2016, **55**, 6651–6656.
32 A. St John, K. I. Goldberg and D. M. Heinekey, in *Organometallic Pincer Chemistry*, ed. G. van Koten and D. Milstein, Springer Berlin Heidelberg, Berlin, Heidelberg, 2013, pp. 271–287.
33 T.-P. Lin and J. C. Peters, *J. Am. Chem. Soc.*, 2013, **135**, 15310–15313.
34 A. Rossin, G. Bottari, A. M. Lozano-Vila, M. Paneque, M. Peruzzini, A. Rossi and F. Zanobini, *Dalton Trans.*, 2013, **42**, 3533–3541.
35 D. Han, M. Joksch, M. Klahn, A. Spannenberg, H. J. Drexler, W. Baumann, H. Jiao, R. Knitsch, M. R. Hansen, H. Eckert and T. Beweries, *Dalton Trans.*, 2016, **45**, 17697–17704.
36 T. J. Hebden, M. C. Denney, V. Pons, P. M. B. Piccoli, T. F. Koetzle, A. J. Schultz, W. Kaminsky, K. I. Goldberg and D. M. Heinekey, *J. Am. Chem. Soc.*, 2008, **130**, 10812–10820.
37 H. C. Johnson, C. L. McMullin, S. D. Pike, S. A. Macgregor and A. S. Weller, *Angew. Chem., Int. Ed.*, 2013, **52**, 9776–9780.
38 A. Johnson, A. J. Martínez-Martínez, S. A. Macgregor and A. S. Weller, *Dalton Trans.*, 2019, **48**, 9776–9781.
39 M. Findlater, K. M. Schultz, W. H. Bernskoetter, A. Cartwright-Sykes, D. M. Heinekey and M. Brookhart, *Inorg. Chem.*, 2012, **51**, 4672–4678.
40 A. Rossin, M. Caporali, L. Gonsalvi, A. Guerri, A. Lledós, M. Peruzzini and F. Zanobini, *Eur. J. Inorg. Chem.*, 2009, **2009**, 3055–3059.
41 R. Kumar and B. R. Jagirdar, *Inorg. Chem.*, 2013, **52**, 28–36.
42 G. Alcaraz, A. B. Chaplin, C. J. Stevens, E. Clot, L. Vendier, A. S. Weller and S. Sabo-Etienne, *Organometallics*, 2010, **29**, 5591–5595.

43 C. J. Stevens, R. Dallanegra, A. B. Chaplin, A. S. Weller, S. A. Macgregor, B. Ward, D. McKay, G. Alcaraz and S. Sabo-Etienne, *Chem. – Eur. J.*, 2011, **17**, 3011–3020.
44 Y. Gloaguen, G. Bénac-Lestrille, L. Vendier, U. Helmstedt, E. Clot, G. Alcaraz and S. Sabo-Etienne, *Organometallics*, 2013, **32**, 4868–4877.
45 T. M. Douglas, A. B. Chaplin, A. S. Weller, X. Yang and M. B. Hall, *J. Am. Chem. Soc.*, 2009, **131**, 15440–15456.
46 A. J. Martínez-Martínez and A. S. Weller, *Dalton Trans.*, 2019, **48**, 3551–3554.
47 W. H. Bernskoetter, C. K. Schauer, K. I. Goldberg and M. Brookhart, *Science*, 2009, **326**, 553.
48 M. L. H. Green and G. Parkin, in *The Chemical Bond III: 100 years old and getting stronger*, ed. D. M. P. Mingos, Springer International Publishing, Cham, 2017, pp. 79–139.
49 A. J. Martínez-Martínez, B. E. Tegner, A. I. McKay, A. J. Bukvic, N. H. Rees, G. J. Tizzard, S. J. Coles, M. R. Warren, S. A. Macgregor and A. S. Weller, *J. Am. Chem. Soc.*, 2018, **140**, 14958–14970.
50 J. Yang, P. S. White, C. K. Schauer and M. Brookhart, *Angew. Chem., Int. Ed.*, 2008, **47**, 4141–4143.
51 M. Roselló-Merino, R. J. Rama, J. Díez and S. Conejero, *Chem. Commun.*, 2016, **52**, 8389–8392.
52 Y. Kawano, T. Kakizawa, K. Yamaguchi and M. Shimoi, *Chem. Lett.*, 2006, **35**, 568–569.
53 A. G. Algarra, L. J. Sewell, H. C. Johnson, S. A. Macgregor and A. S. Weller, *Dalton Trans.*, 2014, **43**, 11118–11128.
54 R. N. Perutz and S. Sabo-Etienne, *Angew. Chem., Int. Ed.*, 2007, **46**, 2578–2592.
55 A. B. Chaplin and A. S. Weller, *Organometallics*, 2011, **30**, 4466–4469.
56 L. K. Krannich, C. L. Watkins, D. K. Srivastava and R. K. Kanjolia, *Coord. Chem. Rev.*, 1992, **112**, 117–129.
57 H. Nöth and H. Vahrenkamp, *Chem. Ber.*, 1967, **100**, 3353–3362.
58 P. Bellham, M. S. Hill, G. Kociok-Köhn and D. J. Liptrot, *Chem. Commun.*, 2013, **49**, 1960–1962.
59 Adapted from: G. B. Fisher, J. C. Fuller, J. Harrison, S. G. Alvarez, E. R. Burkhardt, C. T. Goralski and B. Singaram, *J. Org. Chem.*, 1994, **59**, 6378–6385.
60 S. P. Semproni, C. Milsmann and P. J. Chirik, *J. Am. Chem. Soc.*, 2014, **136**, 9211–9224.
61 L. M. Guard, T. J. Hebden, D. E. Linn and D. M. Heinekey, *Organometallics*, 2017, **36**, 3104–3109.
62 M. Feller, U. Gellrich, A. Anaby, Y. Diskin-Posner and D. Milstein, *J. Am. Chem. Soc.*, 2016, **138**, 6445–6454.
63 W. D. Bailey, W. Kaminsky, R. A. Kemp and K. I. Goldberg, *Organometallics*, 2014, **33**, 2503–2509.
64 M. C. Haibach, D. Y. Wang, T. J. Emge, K. Krogh-Jespersen and A. S. Goldman, *Chem. Sci.*, 2013, **4**, 3683–3692.
65 M. A. Esteruelas, M. Oliván and A. Vélez, *Inorg. Chem.*, 2013, **52**, 5339–5349.
66 L. M. Martínez-Prieto, C. Melero, D. del Río, P. Palma, J. Cámpora and E. Álvarez, *Organometallics*, 2012, **31**, 1425–1438.
67 R. Johansson and O. F. Wendt, *Organometallics*, 2007, **26**, 2426–2430.
68 N. V. Belkova, L. M. Epstein, O. A. Filippov and E. S. Shubina, *Chem. Rev.*, 2016, **116**, 8545–8587.
69 T. D. Forster, H. M. Tuononen, M. Parvez and R. Roesler, *J. Am. Chem. Soc.*, 2009, **131**, 6689–6691.
70 H. Helten, B. Dutta, J. R. Vance, M. E. Sloan, M. F. Haddow, S. Sproules, D. Collison, G. R. Whittell, G. C. Lloyd-Jones and I. Manners, *Angew. Chem., Int. Ed.*, 2013, **52**, 437–440.
71 J. Spielmann, D. Piesik, B. Wittkamp, G. Jansen and S. Harder, *Chem. Commun.*, 2009, 3455–3456.
72 P. Bellham, M. D. Anker, M. S. Hill, G. Kociok-Köhn and M. F. Mahon, *Dalton Trans.*, 2016, **45**, 13969–13978.
73 M. D. Walter, P. S. White, C. K. Schauer and M. Brookhart, *J. Am. Chem. Soc.*, 2013, **135**, 15933–15947.
74 The $^{31}P\{^{1}H\}$ NMR chemical shift of Ir(PONOP)H has been reported in ESI in ref. 73, the synthesis of which comes from β-elimination from Ir(PONOP)Et. While Rh(PONOP)Et was also structurally characterised its stability towards β-elimination was not reported.
75 C. L. Bailey, A. Y. Joh, Z. Q. Hurley, C. L. Anderson and B. Singaram, *J. Org. Chem.*, 2016, **81**, 3619–3628.
76 G. Barozzino Consiglio, P. Queval, A. Harrison-Marchand, A. Mordini, J.-F. Lohier, O. Delacroix, A.-C. Gaumont, H. Gérard, J. Maddaluno and H. Oulyadi, *J. Am. Chem. Soc.*, 2011, **133**, 6472–6480.
77 C. A. Jaska and I. Manners, *J. Am. Chem. Soc.*, 2004, **126**, 9776–9785.
78 Under these conditions a small amount (~20%) of a new species identified as $[Rh(PONOP)(NMe_2H)][BAr^F{}_4]$ was also observed, δ 198.2 [J(RhP) = 151 Hz]. This does not react with $H_3B{\cdot}NMe_3$ and we have not observed it in any other experiments – suggesting that it does not play a role in catalysis.
79 A. A. Mikhailine, M. I. Maishan, A. J. Lough and R. H. Morris, *J. Am. Chem. Soc.*, 2012, **134**, 12266–12280.
80 J. Burés, *Angew. Chem., Int. Ed.*, 2016, **55**, 2028–2031.
81 J. Burés, *Angew. Chem., Int. Ed.*, 2016, **55**, 16084–16087.
82 V. Vasilenko, C. K. Blasius and L. H. Gade, *J. Am. Chem. Soc.*, 2018, **140**, 9244–9254.
83 M. J. Hynes, *J. Chem. Soc., Dalton Trans.*, 1993, 311–312.
84 T. A. Shuttleworth, M. A. Huertos, I. Pernik, R. D. Young and A. S. Weller, *Dalton Trans.*, 2013, **42**, 12917–12925.
85 X. Chen, J.-C. Zhao and S. G. Shore, *Acc. Chem. Res.*, 2013, **46**, 2666–2675.
86 M. A. Fox, A. E. Goeta, A. K. Hughes and A. L. Johnson, *J. Chem. Soc., Dalton Trans.*, 2002, 2132–2141.
87 Mechanisms involving B–H and N–H activation at the Rh centre entailed significantly higher barriers – see ESI.‡
88 The energy of 3-coordinate $[Rh(PONOP)]^+$ (+17.5 kcal mol^{-1}) suggests a purely dissociative mechanism is less favourable.
89 In comparison the computed dipole for $\mathbf{TS(3\text{-}4)_B}$ is 9.1 D and for $\mathbf{3}{\cdot}NMe_2H$ 6.3 D. $\mathbf{TS(3\text{-}4)_N}$ remains more stable in the absence of the solvent correction, but only by 0.5 kcal mol^{-1}.
90 An alternative pathway involving stepwise B–H and N–H activation was also characterised but this has a higher barrier of 34.2 kcal mol^{-1}.

91 M. Espinal-Viguri, S. E. Neale, N. T. Coles, S. A. Macgregor and R. L. Webster, *J. Am. Chem. Soc.*, 2019, **141**, 572–582.
92 K. Kirchner, N. Gorgas, B. Stöger and L. F. Veiros, *Angew. Chem., Int. Ed.*, 2019, DOI: 10.1002/anie.201906971.
93 A. B. Pangborn, M. A. Giardello, R. H. Grubbs, R. K. Rosen and F. J. Timmers, *Organometallics*, 1996, **15**, 1518–1520.
94 O. J. Metters, A. M. Chapman, A. P. M. Robertson, C. H. Woodall, P. J. Gates, D. F. Wass and I. Manners, *Chem. Commun.*, 2014, **50**, 12146–12149.
95 A. L. Colebatch, B. W. Hawkey Gilder, G. R. Whittell, N. L. Oldroyd, I. Manners and A. S. Weller, *Chem. – Eur. J.*, 2018, **24**, 5450–5455.
96 M. E. Sloan, A. Staubitz, T. J. Clark, C. A. Russell, G. C. Lloyd-Jones and I. Manners, *J. Am. Chem. Soc.*, 2010, **132**, 3831–3841.
97 G. M. Adams, F. M. Chadwick, S. D. Pike and A. S. Weller, *Dalton Trans.*, 2015, **44**, 6340–6342.
98 A. T. Lubben, J. S. McIndoe and A. S. Weller, *Organometallics*, 2008, **27**, 3303–3306.
99 ToC graphic prepared using: J. McFarlane, B. Henderson, S. Donnecke and J. S. McIndoe, An Information-Rich Graphical Representation of Catalytic Cycles, *ChemRxiv*, 2019, DOI: 10.26434/chemrxiv.8206637.v1. Preprint.